Journal of Materials Chemistry A

Accepted Manuscript

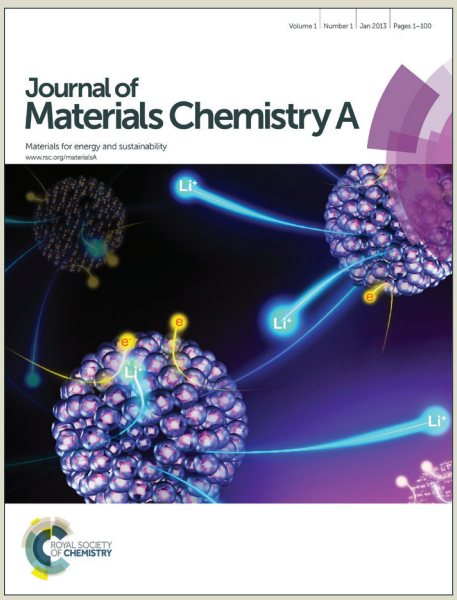

ROYAL SOCIETY OF CHEMISTRY

www.rsc.org/materialsA

Cite this: DOI: 10.1039/c0xx00000x

ARTICLE TYPE

www.rsc.org/xxxxxx

Fabrication of the (Y_2O_3: Yb-Er)/Bi_2S_3 Composite Film for Near-Infrared Photoresponse

Hong Jia[a], Chen ping[a], Cheng Xu[a], Jiajia Zhou[b], Xiangwen Sang[a], Juechen Wang[a], Chang Liu[a], Xiaofeng Liu[a]* and Jianrong Qiu[a,c]*

Received (in XXX, XXX) Xth XXXXXXXXX 20XX, Accepted Xth XXXXXXXXX 20XX

DOI: 10.1039/b000000x

Harvest of near infrared (NIR) radiation in photovoltaic devices is highly desirable as it is recognized as a potential pathway to break the Shockley–Queisser limit of solar conversion efficiency. Here, (Y_2O_3: Yb-Er)/Bi_2S_3 composite films with photoactive current generation under NIR light excitation were fabricated by a simple electro-deposition and successive ionic layer adsorption and reaction (SILAR) method. The composite films consist of homogeneous crystalline particles of the Y_2O_3 with a lamellar morphology covered by Bi_2S_3 nanoparticles. Upon excitation by a 980 nm laser, the Y_2O_3: Yb-Er layer in the composite film converts NIR photons into visible emission through upconversion, which is absorbed by the covered Bi_2S_3 nanoparticles and leads to the generation of photoelectrons. With the use of a standard electrochemical cell where the composite film serves as the photoanode, we demonstrate robust photocurrent generation in aqueous solution. This study suggests a promising strategy for the harvesting of NIR radiation in solar cell, photocatalysts, and infrared photo-detectors.

1 Introduction

In recent years, hybrid structures have attracted growing interest due to their flexibility and extendable properties.[1,2] Multicomponent hybrid materials containing two or more components often exhibit multiple functionalities far beyond those of the individual component, thus providing a promising strategy for nanoscale engineering of optoelectronic, photocatalysts and photovoltaic (PV) devices.[3-8] Since the 20th century, the conversion of solar radiation directly to electric energy has become reality by solar cells based on semiconductors of different characteristics, such as silicon and TiO_2. However, semiconductor itself only absorbs light photons with energy higher than the band gap. In other words, solar radiation of sub-band gap energy, mostly near infrared (NIR) light, cannot be used and therefore do not contribute to photocurrent generation in PV devices.[9-15] This fact has long limited the power conversion efficiency of conventional solar cells. Breaking this limit could be possible if new hybrid materials allow the efficient utilization of NIR radiation.

Recently, it was reported that the conversion efficiency of solar cells can be improved by adding an up-conversion (UC) layer at the rear face of PV device.[16-18] In these semiconductor-UC hybrid structures, the UC layer generates visible emissions which are then absorbed by the semiconductor and finally produce additional photocurrent. Rare earth (RE) ions activated inorganic compounds, such as oxide and fluoride, are often used as UC materials due to their bright emission and chemical robustness.[19-21] In the UC phosphors activated with RE ions, such as Tm^{3+}, Er^{3+}, Ho^{3+}, Nd^{3+}, and Pr^{3+}, UC emission covering the whole visible spectrum can be produced; and the combination of a UC phosphor with a semiconductor with an appropriate band gap would lead to the response to NIR light.

In order to fully absorb the visible UC emission from the RE ions, semicondoctors with absorption edges in the UV or visible (such as TiO_2, CdS or CdSe) are excluded. The ideal choice seem to be again silicon which has a suitable band gap and is in fact the most popular semiconductor working in solar cells. However, silicon with high quality is not ammenable to wet chemistry process under ambient conditions due to its strong covalent bonding. Among different type of semiconductors, bismuth sulfide (Bi_2S_3) is a p-type semiconductor that absorbs almost the whole spectrum of visible light due to its small band gap around 1.3 eV~1.7 eV (729~953 nm). Besides, Bi_2S_3 as a binary semiconductor with a lamellar structure has broad applications in solar cells, switching devices and thermoelectrics.[22-30] Herein, Bi_2S_3 nanoparticles were combined with a UC phosphor of Y_2O_3: Yb-Er for the harvesting of NIR light. The hybrid structure was fabricated by an electro-deposition process, followed by a simple successive ionic layer adsorption and reaction (SILAR) method for the deposition of Bi_2S_3 nanoparticles. We show that the (Y_2O_3: Yb-Er)/Bi_2S_3 film shows strong UC emission from Er^{3+}, which leads to the photocurrent generation under NIR irradiation. The UC phosphor-semiductor juction as well as the fabrication methodology demonstrtaed here may have strong implications for the desigining of NIR-light harvesting PV device and the detection of the NIR light.

The experimental set up as well as the energy transfer mechanism is briefly sketched in Figure 1. In the fabrication process, Y_2O_3: Yb-Er film was first deposited on the photoelectrode (ITO) and then annealed at 600 °C for 2 hours, and finally covered by the SILAR process with a layer of Bi_2S_3 nanoparticles which serve as the absorber for the visible and UV light. For the photocurrent measurement, a conventional three-electrode set-up was used, where the (Y_2O_3: Yb-Er)/Bi_2S_3 film, platinum foil and Ag/AgCl electrode were used as the working electrode (photoanode), counter electrode and the reference electrode, respectively. When irradiated by NIR light at 980 nm, green and red emission are

produced Yb-Er ions pair doped in the Y_2O_3 layer. Yb-Er codoped compounds have been widely employed for generation of UC emissions in both bulk and nanoscale systems,[31-33] where Yb^{3+} ion serves as the sensitizer for the 980 nm light. Due to efficient sensitization by Yb^{3+}, strong visible emissions around 563 nm and 661 nm is generated from the transitions of Er^{3+} ions by $^2H_{11/2}+^4S_{3/2}\rightarrow{}^4I_{15/2}$ and $^4F_{9/2}\rightarrow{}^4I_{15/2}$, respectively (Figure 1b). The visible UC emissions are then fully absorbed by the Bi_2S_3 layer, resulting in the injection of electrons into the ITO photoanode. Based on a photoelectrochemical process, this hybrid film efficiently converts NIR light into electrical energy. The generation of photocurrent by NIR light irradiation is originated from the efficient excitation of Bi_2S_3 by the visible UC emissions, as shown in Figure 1b.

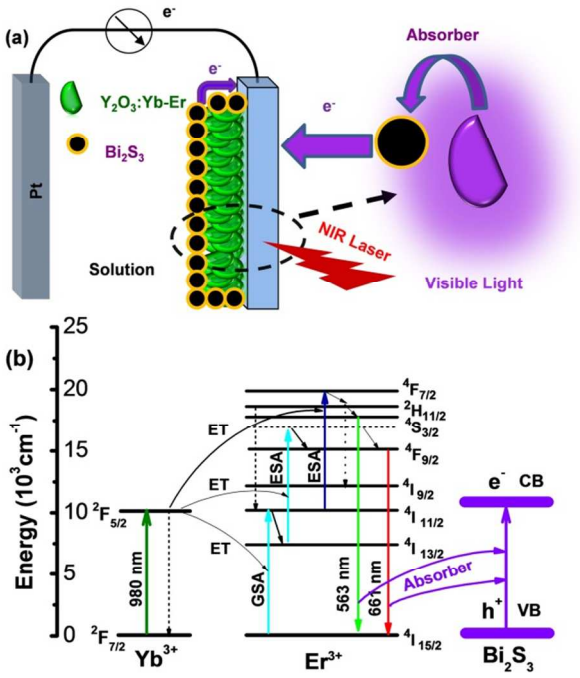

Figure 1. (a) Schematic representation of the fabrication process for the composite thin film of (Y_2O_3: Yb-Er)/Bi_2S_3. (b) Energy diagram where energy transfer process and emission process are indicated for the composite film of (Y_2O_3: Yb-Er)/Bi_2S_3.

2 Experimental

2.1 Thin film synthesis by electro-deposition

Thin films of the Y_2O_3:Yb-Er were grown on indium tin oxide (ITO) coated glass by an electro-deposition process and successive annealing as reported in reference.[34] In a typical process, different amounts of 99.99% purity $Y(NO_3)_3$, $Yb(NO_3)_3$ and $Er(NO_3)_3$ were dissolved in deionized water respectively to get a 0.1M solutions. These solutions were mixed with volume ratio of $V_{Y(NO3)3}$:$V_{Yb(NO3)3}$:$V_{Er(NO3)3}$=X:Y:Z and the mixed solution containing were used as the precursor solution for electro-deposition. All samples were electro-deposited in a standard three-electrode cell, in which working electrode was an ITO coated glass (sheet resistance: 20 Ω/□, purchased from Xiangcity Technology Ltd., China), a platinum foil and Ag/AgCl/saturated KCl was used as a counter electrode and a reference electrode, respectively. Each sample was deposited at 60 °C for 20 min. The applied potential was -1.2 V vs Ag/AgCl/saturated KCl. After the deposition, all the samples were cleaned and dried in air at 60 °C for 2 h, and then annealed at various temperatures (300 °C, 400 °C, 500 °C, 550 °C, 600 °C, 650 °C, 680 °C) for 2.5 h in air.

Bi_2S_3 film was prepared with a simple successive ionic layer adsorption and reaction (SILAR) method. First, 0.005M $Bi(NO_3)_3$•5 H_2O (purity: 99%) solution and 0.008 M Na_2S (purity: 98%) solution were prepared in separate glass beakers with deionized water. Secondly, the ITO glass was immersed in the $Bi(NO_3)_3$ solution for 10 s to absorb a large number of Bi^{3+} and NO_3^- ions. The weakly bounded ions were removed by rinsing the substrate in deionized water for 15 s again. The adsorbed Bi^{3+} ions react with S^{2-} when the substrate is immersed in the Na_2S solution for 10 s. Finally, the substrate was rinsed by in deionized water for 15 s to dissove the unreacted ions, leaving only the Bi_2S_3 nanoparticals in the substrat. Finally, the Bi_2S_3 film was dried at 60 °C in oven for 30 min.

Scheme 1 is the schematic for preparation of the (Y_2O_3: Yb-Er)/Bi_2S_3 composite films, Y_2O_3: Yb-Er film was deposited first on the ITO substrate as described above, and then, a Bi_2S_3 layer of varying thickness was coated onto the Y_2O_3: Yb-Er film by several cycles of SLAR reaction.

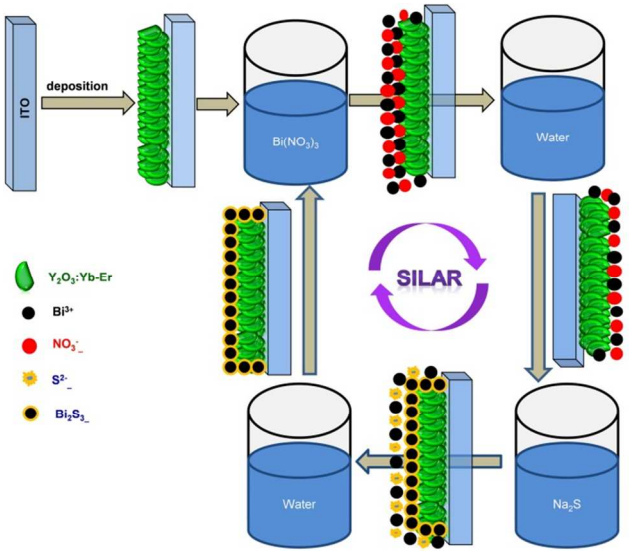

Scheme 1. Schematic illustration for preparation of (Y_2O_3: Yb-Er)/Bi_2S_3 composite film

2.2 Characterizations

Crystal structure for the thin film samples was examined with X-ray diffraction (XRD) by a RIGAKU D/MAX 2550/PC system using Cu K_α radiation. Microstructures of the samples were examined with a Hitachi S-4800 scanning electron microscope. TG and DTA measurements were performed with the TGA7 and DTA7 (Perkin Elmer Co. Ltd., USA)) system at a heating rate of 10 °C/min. UV-Vis diffuse reflectance spectra of the films were measured at room temperature on a Hitachi-4100 spectrophotometer. The UC luminescence of the samples was measured using a FLS920 fluorescence spectrophotometer (Edinburgh Instrument Ltd., U. K.) using a 980 nm laser diode (1 W) as the excitation. Photocurrent density was measured with a CHI 600C electrochemical station using the same three-electrode cell as described previously. Na_2SO_4 solution (0.5 M) was use as the electrolyte solution and a 980 nm laser diode (1 W) was employed as the NIR light source.

3 Results and discussion

3.1 Structural properties

In our experiment, the Y_2O_3: Yb-Er thin films were prepared using a two-step process: electro-deposition and post annealing process. The films show a dominant red UC emission at 661 nm from the transition $^4F_{9/2}\rightarrow{}^4I_{15/2}$ of Er^{3+} excited by a 980 nm laser diode (Figure 4b and Figure S4). The UC emission intensity of the Y_2O_3: Yb-Er thin films is closely related with the crystal structure of the host material, doping concentration, deposition time, solution concentration and annealing temperature. The film deposited under 0.1 M concentration (20 min, solution with norminal ratio of Y:Yb:Er=96:3:1) and annealing at 600 °C (2.5 h) exhibits the strongest red UC emission (Figure S7). Thereafter, this Y_2O_3: Yb-Er thin film (deposited from solution with Y:Yb:Er=96:3:1) was covered with a layer of Bi_2S_3 nanoparticles by the SILAR process.

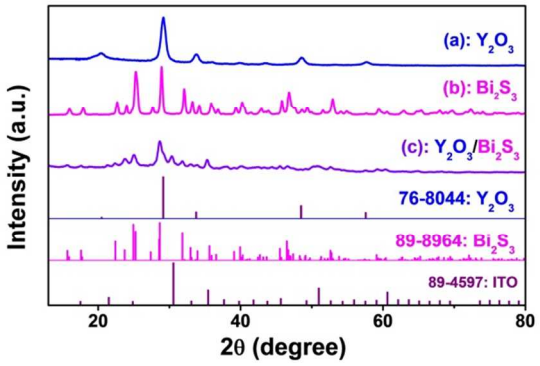

Figure 2. X-Ray diffraction patterns for samples of: (a) the Y_2O_3: Yb-Er thin film, (b) the Bi_2S_3 thin film, (c) the composite film of (Y_2O_3: Yb-Er)/Bi_2S_3.

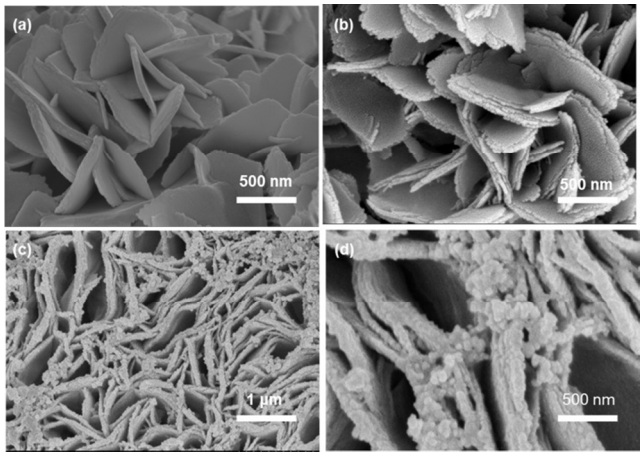

Figure 3. SEM images of thin films: (a) $Y_2(OH)_{5.14}(NO_3)_{0.86}\cdot H_2O$ thin film, (b) the Y_2O_3: Yb-Er thin film, (c) and (d) the composite film of (Y_2O_3: Yb-Er)/Bi_2S_3.

To study the formation of Y_2O_3 film, the samples before and after annealing are shown in Figure S2. For the as-formed film and the films annealed at 300 °C, all the diffraction peaks of can be assigned to $Y_2(OH)_{5.14}(NO_3)_{0.86}\cdot H_2O$ (JCPDS: 32-1435). After annealing at 400 °C, 500 °C and 600 °C, the diffraction peaks assigned to $Y_2(OH)_{5.14}(NO_3)_{0.86}\cdot H_2O$ disappear steadily, while new diffraction peaks from Y_2O_3 emerge (JCPDS: 01-76-8044). Figure 2a shows that the peaks in the XRD patterns of Y_2O_3: Yb-Er film can be all indexed to cubic phase of Y_2O_3 (JCPDS: 01-76-8044), and no other phase can be identified except the substrate ITO (JCPDS card No. 89-4597). Figure S2a and Figure 3a are the cross-section and surface images of the Y_2O_3: Yb-Er thin film without annealing. The film shows a flaky-like surface morphology, and the thickness of the film is about 13.6 μm. After annealing at 600 °C for 2.5 h, the film thickness remains contstant and the similar flaky-like surface morphology is almost preserved in spite of phase transition to pure Y_2O_3. From a closer observation, we can see that the sheet-like structures evolves to a lamellar structure, which may be ascribed to the decomposition of $Y_2(OH)_{5.14}(NO_3)_{0.86}$ and the formation of Y_2O_3, accompanied by the releasing of gases of H_2O, NO_2 and O_2. This decomposition process is also evident in the thermogravimetry (TG) and differential thermal analysis (DTA) curves for the $Y_2(OH)_{5.14}(NO_3)_{0.86}\cdot H_2O$ film (Figure S1). In the composite film where Bi_2S_3 is deposited later onto the Y_2O_3 crystals, the characteristic diffraction peaks of only Bi_2S_3 and Y_2O_3 are detected (Figure 2c), and the Bi_2S_3 nanoparticles formed on the flaky-like surface of the Y_2O_3: Yb-Er thin film are easily observed by SEM images (Figure 3c and Figure 3d). The diffraction peaks of the composite film are strongly reduced as compared to that of pure Y_2O_3 and Bi_2S_3 probably because the layer of Bi_2S_3 particles at surface has lower crystallinity.

3.2 Photoluminescence Properties

Figure 4a shows the reflectance spectra of Y_2O_3: Yb-Er thin film, Bi_2S_3 thin film, and the (Y_2O_3: Yb-Er)/Bi_2S_3 composite film. Due to the small absorption cross section, the f-f transitions of RE ions is not observed in the spectrum for Y_2O_3: Yb-Er film (Figure 4a). For the Bi_2S_3 film, the absorption edge is found at around 950 nm, in agreement with its band gap of 1.3 eV. In comparison, the absorption edge of the (Y_2O_3: Yb-Er)/Bi_2S_3 composite film cannot be clearly located possibly due to increased scattering, while it is clear that the whole visible region can be covered by the (Y_2O_3: Yb-Er)/Bi_2S_3 composite film.

We then compare the UC emissions of the Y_2O_3: Yb-Er thin film with that of the (Y_2O_3: Yb-Er)/Bi_2S_3 composite film under NIR excitation by a 980 nm laser diode (Figure 4b). Green emission bands observed at 531 to 571 nm are associated with the $^2H_{11/2}$, $^4S_{3/2}\rightarrow{}^4I_{15/2}$ transitions of Er^{3+}, while red band centered around 661 nm is associated with the $^4F_{9/2}\rightarrow{}^4I_{15/2}$ transition. These visible emissions are produced as a result of efficient energy transfer from Yb^{3+} to Er^{3+}, as shown in Figure 1b. Different from fluoride host, e. g. $NaYF_4$,[35] the red emission is overwhelming as compared to the green emission, implying that the difference in the phonon energy of the host plays an important role in the UC process. Similarly, dominating red emission is observed in Y_2O_3: Yb-Er nanoparticles, suggesting the probability of phonon-assisted nonradiative relaxation from $^2H_{11/2}$, $^4S_{3/2}$ to $^4F_{9/2}$ is much higher in oxide than that in fluoride.[36] For the composite film, sharp reduction of both emissions (green and red) are observed from (Y_2O_3: Yb-Er)/Bi_2S_3 composite film as compared to the Y_2O_3: Yb-Er film. Furthermore, the red light (661 nm) is weakened further with the increase of the thickness of Bi_2S_3 (accessed by changing a number of cycles for SILAR). In our experiment, the optimal number of cycles for SILAR to deposit Bi_2S_3 onto the Y_2O_3: Yb-Er film was found to be about 80 (Figure 4c). This evidence confirms efficient quenching of UC emission by Bi_2S_3 as a result of energy transfer from Y_2O_3: Yb-Er to Bi_2S_3.

The transfer of enenrgy between these two layers are dominated by a radiative reabsorption process rather than a Föster-Dexter type, as the seperation between most particles are far lager than the critical distance.

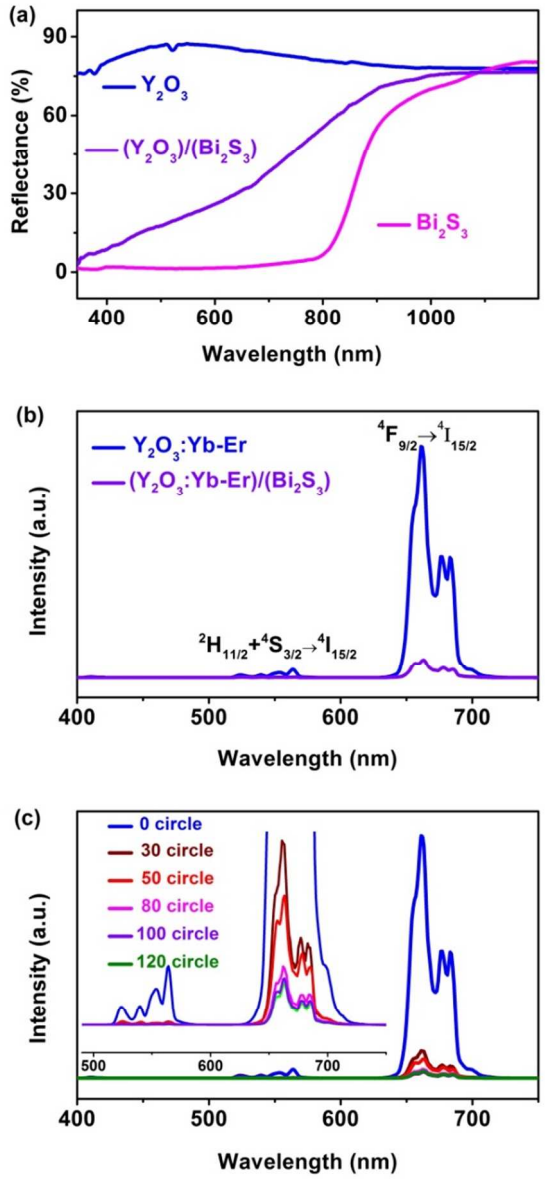

Figure 4. (a) Diffusion reflectance spectra of the Y_2O_3: Yb-Er thin film, the Bi_2S_3 thin film, and the (Y_2O_3: Yb-Er)/(Bi_2S_3) composite film, (b) UC emission spectra of the Y_2O_3: Yb-Er thin film and the composite film of (Y_2O_3: Yb-Er)/(Bi_2S_3). (c) Up-conversion emission spectra of the composite film with different thickness of Bi_2S_3 (accessed by changing the the number of cycles in the SILAR process)

3.3 Photoelectrochemical measurements

As described previously (Figure 1), the conversion of NIR photon to photoelectrons involves the excitation by NIR light, visible UC emissions from the Y_2O_3: Yb-Er thin film, absorption of visible light by the Bi_2S_3 film, and finally electron injection to ITO. The performances of photoelectrochemical cell based on the different films deposited on the ITO photoanodes were evaluated with a standard three-electrode setup under excitation with a 980 nm diode laser. The influence of applied potential on the photocurrent response was investigated by cyclic voltammetry measurements in the potential range of -0.3 V to 0.3 V. Figure 5a shows the photoelectrochemical behaviors of (Y_2O_3: Yb-Er)/Bi_2S_3 composite film. The (Y_2O_3: Yb-Er)/Bi_2S_3 composite film shows notable photocurrent under the 980 nm NIR laser excitation compared to the composite film measured in darkness (Figure 5c), indicating the generation of photoelectrons by the excitation at 980 nm. The photocurrent is produced by Bi_2S_3 as a result of band transition that promotes electrons to its conduction band and the followed charge separation in the electrochemical cell. In comparison, the pure Y_2O_3 film and the Bi_2S_3 film does not show meaningful photocurrent under both 980 nm excitation or in darkness (Figure S8 a and b). This result therefore verifies the proposed energy transfer from Y_2O_3: Yb-Er to Bi_2S_3 (Figure 1).

To examine the contribution of thermal and scattering effect which may have positive effect on photon-current conversion, we prepared another composite film Y_2O_3/Bi_2S_3without rare earth doping. As shown in Figure S8 c, the I-V curves measured in the dark or under 980 nm excited are almost the same for the composite film Y_2O_3/Bi_2S_3, suggesting that the contribution of laser induced heating effect on the photocurrent are negeligibly small. Furthermore, by comparing the I-V curves of Y_2O_3/Bi_2S_3 and pure Bi_2S_3, it becomes clear that the contribution of the scattering by Y_2O_3 particles can be also excluded.

To further confirm the NIR light response, we measured the photocurrent density curves of the (Y_2O_3: Yb-Er)/Bi_2S_3 film (80 cycles for SILAR for Bi_2S_3) under pulsed laser diode excitation (pulse duration: 60 s). A negligible current is observed in darkness at the bias of 0.3 V probably due to surface side reactions. Under laser excitation, the photocurrent jumps to 22 μA, and the rectangular shape of the current-time curve suggests fast light response. In comparison, negative current (about -1.75 μA) was observed at an applied potential of -0.3 V in darkness and this current increases to about -5.9 μA when the cell is irradiated by the 980 nm laser diode. The fast NIR light response observed here again excludes the contribution of thermal effect on the photocurrent generation.

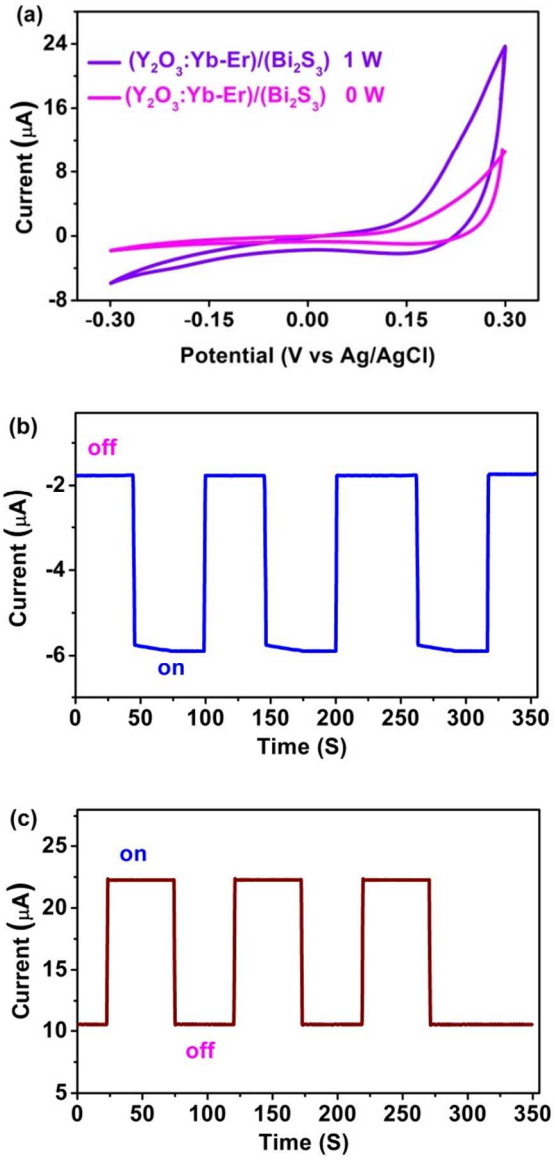

Figure 5. (a) Cyclic voltammetry potentiodynamic behaviors (i. e., I-V curves) of (Y_2O_3: Yb-Er)/Bi_2S_3 composite film measurement in the darkness(0 W) and under excitation by 980 nm laser diode at 1 W. (b, c) Photocurrent response of the composite film at bias potential of -0.3 V(b) and 0.3 V (c).

4 Conclusions

In summary, we designed a (Y_2O_3: Yb-Er)/Bi_2S_3 composite film and fabricated it by electro-deposition and a simple successive ionic layer adsorption and reaction (SILAR) method. In this composite film, NIR light is converted Y_2O_3: Yb-Er to visible photons that excite Bi_2S_3 and produce photoelectrons. With the use of an electrochemical cell, we successfully demonstrated highly photoactive current generation in a photoelectrochemical process driven by NIR irradiation. Combined with the high sensitivity and robust photocurrent generation under NIR light irradiation, the composite film (Y_2O_3: Yb-Er)/Bi_2S_3 demonstrated here may have potential applications in NIR photo-detectors and PV devices.

Acknowledgment

This work was financially supported by the National Natural Science Foundation of China (Grant Nos. 51132004), Fundamental Research Funds for the Central Universities (Grant No. 2014ZP0001), Guangdong Natural Science Foundation (Grant Nos. S2011030001349), National Basic Research Program of China (2011CB808102), Program for Chiangjiang Scholars and Innovative Research Team in University.

Notes and references

[a] *State Key Laboratory of Silicon Materials, School of Materials Science and Engineering, Zhejiang University, Hangzhou 310027, China*
[b] *College of Materials Science and Engineerging, China Jiliang University, Hangzhou 310018, China*
[c] *State Key Laboratory of Luminescent Materials and Devices, South China University of Technology, Guangzhou 510640, China*

1 R. S. Selinsky, Q. Ding, M. S. Faber, J. C. Wright and S. Jin, *Chem. Soc. Rev.,* 2013, **42**, 2963.
2 A. G. Dong, J. Chen, P. M. Vora, J. M. Kikkawa and C. B. Murray, *Nature*, 2010, **466**, 474.
3 W. K. Su, M. M. Zheng, L. Li, K. Wang, R. Qiao, Y. J. Zhong, Y. Hu and Z. Q. Li, *J. Mater. Chem. A., 2014, 2, 13486.*
4 S. Q. Huang, Z. Y. Lou, A. D. Shan, N. W. Zhu, K. L. Feng and H. P. Yuan, *J. Mater. Chem. A.,* 2014, **2**, 16165.
5 N. Pellet, P. Gao, G. Gregori, T. Y. Yang, M. K. Nazeeruddin, J. Maier and M. Gratzel, *Angew Chem. Int. Ed.*, 2014, **53**, 3151.
6 J. D. Wild, A. Meijerink, J. K. Rath, W. G. J. H. M. van Sark and R. E. I. Schropp, *Energy Environ. Sci.,* 2011, **4**, 4835; X. Zhang, H. Huang, J. Liu, Y. Liu and Z. H. Kang, *J. Mater. Chem. A*., 2013, **1**, 11529; S. Q. Huang, L. Gu, C. Miao, Z. Y. Lou, N. W. Zhu, H. P. Yuan and A. D. Shan, *J. Mater. Chem. A*., 2013, **1**, 7874.
7 S. P. Albu, A. Ghicov, J. M. Macak, R. Hahn and P. Schmuki, *Nano Lett.*, 2007, **7**, 1286.
8 X. J. Xu, X. S. Fang, T. Y. Zhai, H. B. Zeng, B. D. Liu, X. Y. Hu, Y. Bando and D. Golberg, Small., 2011, **7**, 445.
9 J. R. Jennings, A. Ghicov, L. M. Peter, P. Schmuki and A. B. Walker, *J. Am. Chem. Soc.*, 2008, **130**, 13364.
10 J. Wang and Z. Q. Lin, *Chem. Mater.*, 2010, **22**, 579.
11 W. J. Lee, J. M. Lee, S. T. Kochuveedu, T. H. Han, H. Y. Jeong, M. Park, J. M. Yun, J. Kwon, K. No, D. H. Kim, S. O. Kim, *ACS Nano*., 2012, **6**, 935.
12 S. Nakabayashi, A. Fujishima and K. Honda, *Chem. Phys. Lett.*, 1983, **102**, 464.
13 A. Fujishima and K. Honda, *Nature.*, 1972, **37**, 238.
14 L. X. Yang, D. M. He, Q. Y. Cai, and C. A. Grimes, J. Phys. Chem. C. 2007, **111**, 8214.
15 J. Y. Zhang, H. L. Zhu, S. K. Zheng, F. Pan and T. M. Wang, *ACS Appl. Mater. Interfaces.,* 2009, **1**, 2111.
16 X. Y. Huang, S. Y. Han, W. Huang and X. G. Liu, *Chem. Soc. Rev.*, 2013, **42**, 173.
17 L. W. Wang, *Energy Environ Sci.*, 2009, **2**, 944; K. Börjesson, D. Dzebo, B. Albinssonb and K. Moth-Poulsen, *J. Mater. Chem. A*., 2013, **1**, 8521.
18 G. B. Shan, H. Assaaoudi and G. P. Demopoulos, *ACS Appl. Mater. Interfaces*., 2011, **3**, 3239.
19 J. A. Capobianco, J. C. Boyer, F. Vetrone, A. Speghini, and M. Bettinelli, *Chem. Mater.*, 2002, **14**, 2915.
20 J. Li, J. H. Zhang, Z. D. Hao, X. Zhang, J. H. Zhao and Y. S. Huo, *Appl. Phys. Lett*., 2012, **101**, 121905.
21 Y. B. Mao, T. Tran, X. Guo, J. Y. Huang, C. K. Shih, K. L. Wang, and J. P. Chang, *Adv. Funct. Mater.*, 2009, **19**, 748.
22 H. F. Cheng, B. B. Huang, X. Y. Qin, X. Y. Zhang and Y. Dai, *Chem. Comm.*, 2012, **48**, 97.
23 X. H. Gao, H. B. Wu, L. X. Zheng, Y. J. Zhong, Y. Hu, X. W. Lou, *Angew. Chem. Int. Ed.*, 2014, **53**. 5917.

24 Z. J. Zhang, W. Z. Wang, L. Wang and S. M. Sun, *ACS Appl. Mater. Interfaces.,* 2012, **4**, 593.

25 H. Bao, C. M. Li, X. Q. Cui, Y. Gan, Q. L. Song, and J. Guo, *Small*, 2008, 4, 1125.

26 L. Cademartiri, F. Scotognella, P. G. O'Brien, B. V. Lotsch, J. Thomson, S. Petrov, N. P. Kherani and G. A. Ozin, *Nano Lett.*, 2009, **9**, 1482.

27 O. Rabin, J. M. Perez, J. Grimm, G. Wojtkiewicz, and R. Weissleder, *Nat. Mater.*, 2006, **5**, 118.

28 G. Manna, R. Bose and N. Pradhan, *Angew Chem. Int. Ed.*, 2014, **53**, 6743.

29 W. S. Liu, C. F. Guo, M. L. Yao, Y. C. Lan, H. Zhang, Q. Zhang, S. Chen, C. P. Opeil, Ren, Z. F. *Nano Energy*, 2014, **4**, 113.

30 C. F. Guo, J. Zhang, Y. Tian and Q. Liu, *ACS Nano*., 2012, **6**, 8746.

31 M. B. Korzenski, P. Lecoeur, B. Mercey, D. Chippaux and B. Raveau, *Chem. Mater.*, 2000, **12**, 3139.

32 J. K. Richard Weber, J. J. Felten, B. Cho and P. C. Nordine, *Nature*, 1998, **393**, 769.

33 G. Glaspell, J. Anderson, J. R. Wilkins and M. S. El-Shall, *J. Phys. Chem. C*., 2008, **112**, 11527.

34 L. Wang, H. Jia, X. Yu, Y. Zhang, P. Du, Z. Xi, and D. Jin, *Electrochem. Solid. ST.* **2010**, *13*, S5-S5.

35 F. Wang, Y. Han, C. S. Lim, Y. H. Lu, J. Wang, J. Xu, H. Y. Chen, C. Zhang, M. H. Hong and X. G. Liu, *Nature*, 2010, **463**, 1061.

36 S. H. Huang, J. Z. Xu, G. Zhang, X. Zhang, L. Z. Wang, S. L. Gai, F. He, N. Niu, M. L. Zhang and P. P. Yang, *J. Mater. Chem.*, 2012, **22**, 16136.